A General Model for Analyzing the Thermal Characteristics of a Class of Latent Heat Thermal Energy Storage Systems

Kang Yanbing

Zhang Yinping*

Jiang Yi

Zhu Yingxin

Department of Thermal Engineering,
Tsinghua University,
Beijing, 100084, P.R. China

The present study describes and classifies latent heat thermal energy storage (LHTES) systems according to their structural characteristics. A general model is developed for analyzing the thermal characteristics of the various typical LHTES systems to simulate thermal characteristics such as instantaneous heat transfer rate, instantaneous thermal storage capacity, etc. of the various typical LHTES systems. The model can calculate some important but difficult to measure system parameters for monitoring the charging or discharging processes of the systems. The model is verified using experimental data in the literature. Results from the model can be used to discuss the influence of the characteristic geometric parameters of LHTES units, the physical properties of the phase change material (PCM), the flow type and the velocity of heat transfer fluid (HTF) on the system thermal performance and to identify the key factors influencing the system thermal performance. The general model can be used to select and optimize the system structure and to simulate the thermal behavior of various typical LHTES systems.

1 Introduction

Efficiency and environmental concerns have increased the importance of thermal energy storage (TES) systems in such fields as solar energy systems, greenhouses and power plants. Thermal energy storage systems can improve system management and can help match supply and demand patterns. Among the available technologies for thermal storage systems, latent heat thermal energy storage (LHTES) systems can store a great amount of thermal energy in a small volume with a relatively small temperature variation. Recently, for the purpose of effective load leveling of electric power system, much attention has been given to cool storage air-conditioning systems.

Many theoretical studies concerning the thermal characteristics of LHTES systems have been undertaken. Brousseau and Lacroix [1] studied the thermal performance of a multi-layer PCM storage unit. Cao and Faghri [2–4] numerically analyzed the thermal performance of a shell-and-tube PCM storage unit using the enthalpy transform model. Esen and Durmus [5] studied inward and outward solidification in a tube-and-shell LHTES system. Egolf [6] and Homma et al. [7] studied the heat transfer characteristics of spherical latent heat storage capsules. Arnold [8, 9] developed a correlation for the effective heat transfer coefficient for ice-storage (where the ice is contained in spherical capsules) using theoretical analysis and experiment data to effectively simulate the system thermal performance. Since those researchers all focused on the thermal performance of a specific type of LHTES, the applicable range of their models is quite limited. In fact, many LHTES systems used in practical applications which at first seem to be different, share common features from the heat transfer point of view. The present work will (1) identify the common features of various LHTES systems often used in practical applications; (2) build a general model capable of analyzing the thermal characteristics of various LHTES systems and (3) determine the key factors which influence the thermal performance of the systems.

* Corresponding author.

Contributed by the Solar Energy Division of THE AMERICAN SOCIETY OF MECHANICAL ENGINEERS for publication in the ASME JOURNAL OF SOLAR ENERGY ENGINEERING. Manuscript received by the ASME Solar Energy Division, Aug. 1999; final revision, Nov. 1999. Associate Technical Editor: M. Olszewski.

2 Classification and the Common Features of Typical LHTES Systems

Typical LHTES systems used in engineering applications can be classified based on their structural characteristics as packed bed systems or shell-and-tube systems. For packed bed systems, the PCM container can be spherical, rectangular, cylindrical, etc. The systems can also be divided according to the flow type as internal flow or external flow (including parallel flow and cross flow). Flat-plate structures and shell-and-tube structures with internal flow are outward phase change systems, while shell-and-tube structures with parallel flow or cross flow and spherical packed bed are inward phase change systems. Some typical LHTES systems often used in engineering applications are shown in Figs. 1 and 2. The systems all have PCM or uniform PCM capsules distributed uniformly in the system. The heat transfer in each system is two-dimensional conduction with solid-liquid phase change and an unknown fluid temperature variation along the axial direction. The PCM thermal resistance and the effective heat transfer area both vary with time and space. The analysis of the different type of LHTES differs in the value of some characteristic parameters, such as characteristic dimension, thermal resistance, etc. All systems share common features as summarized in Fig. 3. The parameters for the various systems in the figure are listed in Tables 1 and 2.

3 General Model of Solid-Liquid LHTES Systems

The analysis is simplified by assuming:

(1) Axial conduction in the PCM is negligible.
(2) Ste $\ll 1$, which means that the sensible thermal storage capacity can be neglected compared with latent thermal storage capacity.
(3) The HTF capacitance can be ignored.
(4) Natural convective heat transfer in the liquid PCM is neglected.
(5) For inward phase change structures, $L \gg r_o$.

3.1 General Heat Transfer Model of Solid-Liquid LHTES Systems. The energy equation for the PCM is

$$H_m \cdot \rho_p \cdot \frac{\partial A_{c,p}(t, x)}{\partial t} = U \cdot P \cdot |T_f(t, x) - T_m| \qquad (1)$$

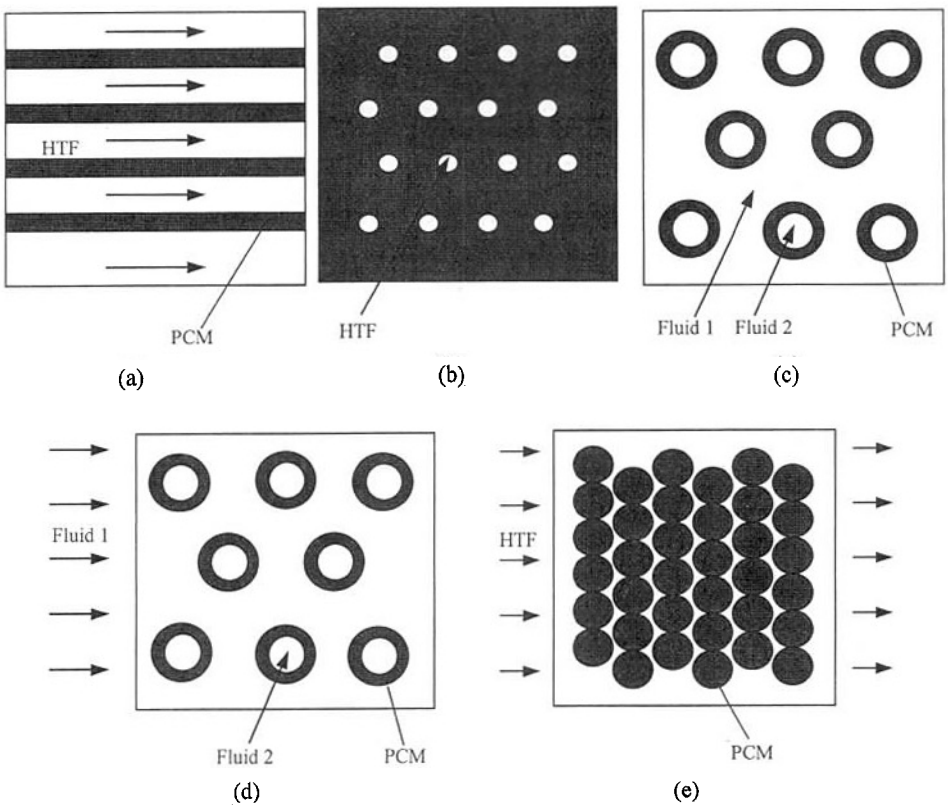

Fig. 1 Schematics of typical LHTES systems (*a*) Flat-plate (*b*) Shell-and-tube with internal flow (*c*) Shell-and-tube with parallel flow (*d*) Shell-and-tube with cross flow (*e*) Sphere packed bed

Where $A_{c,p}$ is the area that has experienced phase change which is the solid area in a freezing process and the liquid area in a melting process. The energy equation for the HTF is

$$\dot{m}_f \cdot c_{p,f} \cdot \frac{\partial T_f(t, x)}{\partial x} = -U \cdot P \cdot (T_f(t, x) - T_m) \tag{2}$$

where,

$$U = h_f \cdot R_r \tag{3}$$

and

$$R_r = \frac{R_f}{R_f + R_w + R_p}, \tag{4}$$

subject to the initial conditions

$$A_{c,p}\ (t = 0, x) = A_{c,p,0}(x), \quad T_f\ (t = 0, x) = T_{f,0}$$

and the boundary condition

Nomenclature

A = overall heat transfer area, m^2
$A_{c,p}$ = cross sectional area over which phase change has occurred, m^2
A_c = cross sectional area of LHTES system, m^2
Bi = Biot number
c_p = specific heat, J kg^{-1} K^{-1}
Fo = Fourier number
F_r = molten/frozen PCM mass fraction
h_f = convective heat transfer coefficient, W m^{-2} K^{-1}
H_m = heat of fusion, J kg^{-1}
HTF = heat transfer fluid
k = thermal conductivity, W m^{-1} K^{-1}
L = length, m
$\dot{m}_f$ = heat transfer fluid mass flow rate, kg s^{-1}
NTU = number of transfer units
P = wetted perimeter of fluid duct, heat transfer area unit length, m
q = heat transfer rate, W
Q = thermal storage capacity, J
r = radius, m
R = thermal resistance, W^{-1} m^2 K
Ste = Stefan number
t = time, s
T_f = heat transfer fluid temperature, K
T_m = PCM melting temperature, K
U = overall heat transfer coefficient, W m^{-2} K^{-1}
v_f = heat transfer fluid velocity, m s^{-1}
V = volume, m^3
W = width, m
x = axial coordinate, m

Greek Symbols

ρ = density, kg m^{-3}
δ = thickness, m
ϵ = LHTES system porosity
Φ = structural thermal resistance coefficient
η = coordinate of phase change interface or fluid duct, see Fig. 3, m

Subscripts

ave = average
eff = effective
f = fluid, fin
i = inside
in = inlet
max = maximum
o = outside
out = outlet
p = PCM
w = wall

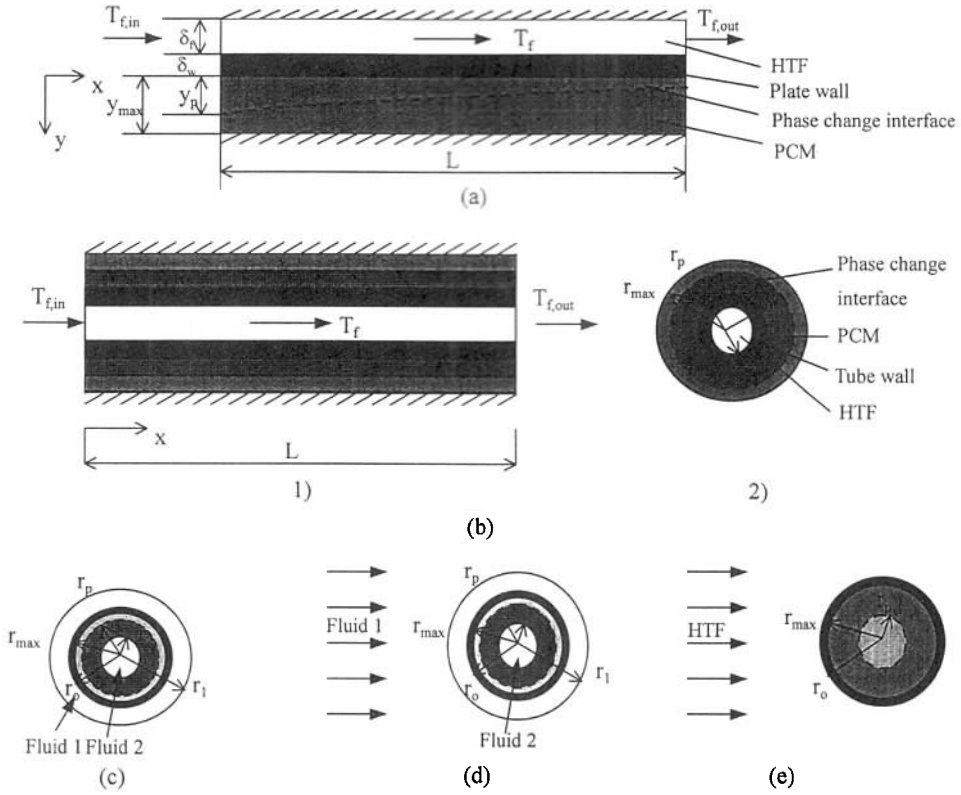

Fig. 2 Cell parameters for typical LHTES systems (*a*) Flat-plate (*b*) Shell-and-tube with internal flow: 1) Longitudinal section 2) Cross section (*c*) Shell-and-tube with parallel flow (*d*) Shell-and-tube with cross flow (*e*) Sphere packed bed

$$T_f\,(t,\,x=0)=T_{f,in}(t).$$

R_f is the convective heat transfer thermal resistance between the HTF and the wall of the PCM cell, R_w is the thermal conduction resistance of the wall and R_p is the thermal conduction resistance of the solidified/melt portion of the PCM.

The analysis of the LHTES systems can be simplified using the following dimensionless parameters

$$\theta_f=\frac{T_f-T_m}{T_{f,in}-T_m},\quad \bar{A}_{c,p}=\frac{A_{c,p}}{A_{c,\max}},\quad \mathrm{Fo}=\frac{a_p t}{A_{c,\max}},\quad X=\frac{x}{L},$$

$$\mathrm{Ste}=\frac{c_{p,p}|T_m-T_{in}|}{H_m},\quad \mathrm{NTU}=\frac{h_f A}{\dot{m}_f c_{p,f}},\quad \mathrm{Bi}=\frac{h_f P}{k_p},$$

$$\Phi=\frac{R_w+R_p}{R_f\cdot\mathrm{Bi}}$$

where,

$$a_p=\frac{k_p}{\rho_p c_{p,p}},\quad R_r=\frac{R_f}{R_f+R_w+R_p}=f(\mathrm{Bi},\,\bar{A}_{c,p})=\frac{1}{1+\mathrm{Bi}\cdot\Phi}$$

$\theta_f(\mathrm{Fo},X)$ and $\bar{A}_{c,p}(\mathrm{Fo},X)$ are determined from the solution of the governing equations. The dimensionless parameters can be used to transform equations (1)-(4) into dimensionless equations

$$\frac{\partial\bar{A}_{c,p}(\mathrm{Fo},X)}{\partial\mathrm{Fo}}=\mathrm{Ste}\cdot\mathrm{Bi}\cdot R_r(\mathrm{Fo},X)\cdot|\theta_f(\mathrm{Fo},X)| \tag{5}$$

$$\frac{\partial\theta_f(\mathrm{Fo},X)}{\partial X}=-\mathrm{NTU}\cdot R_r(\mathrm{Fo},X)\cdot\theta_f(\mathrm{Fo},X) \tag{6}$$

Subject to the initial conditions

$$\bar{A}_{c,p}\,(\mathrm{Fo}=0,\,X)=\bar{A}_{c,p,0}(X),\quad \theta_f\,(\mathrm{Fo}=0,\,X)=\frac{T_{f,0}-T_p}{T_{f,in}-T_p}$$

and the boundary condition

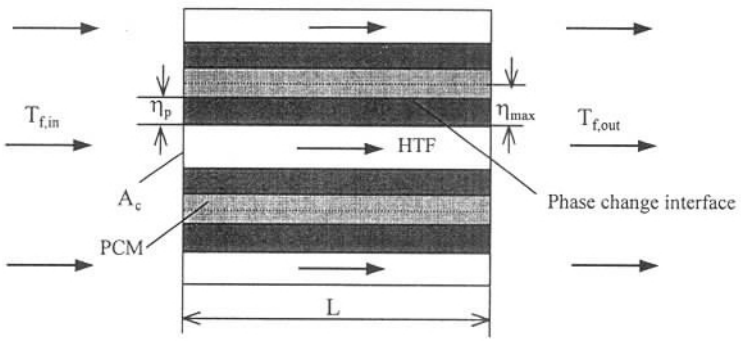

Fig. 3 Schematic of general LHTES system

Table 1 Characteristic parameters for each system used in the general model

General model	Fig. 3	η_p	$\bar{A}_{c,p} = \frac{A_{c,p}}{A_{c,\max}}$	$A_{c,\max}$	P	Φ
Flat-plate	Fig. 1(*a*) Fig. 2(*a*)	y_p	$\frac{y_p}{y_{\max}}$	$W \cdot y_{\max}$	W	$\frac{k_p \cdot \delta_w}{k_w \cdot W} \cdot \frac{y_{\max}}{W} \bar{A}_{c,p}$
Shell-and-tube with internal flow	Fig. 1(*b*) Fig. 2(*b*)	r_p	$\frac{r_p^2 - r_o^2}{r_{\max}^2 - r_o^2}$	$\pi(r_{\max}^2 - r_o^2)$	$2\pi \cdot r_i$	$\frac{1}{2\pi}\left(\frac{k_p}{k_w}\ln\frac{r_o}{r_i} + \frac{1}{2}\ln\left(\bar{A}_{c,p}\cdot\left(\left(\frac{r_{\max}}{r_o}\right)^2 - 1\right) + 1\right)\right)$
Shell-and-tube with parallel flow	Fig. 1(*c*) Fig. 2(*c*)	r_p	$\frac{r_{\max}^2 - r_p^2}{r_{\max}^2 - r_2^2}$	$\pi(r_{\max}^2 - r_2^2)$	$2\pi \cdot r_o$	$\frac{1}{2\pi}\left(\frac{k_p}{k_w}\ln\frac{r_o}{r_{\max}} - \frac{1}{2}\ln\left(1 - \bar{A}_{c,p}\cdot\left(1 - \left(\frac{r_2}{r_{\max}}\right)^2\right)\right)\right)$
Shell-and-tube with cross flow	Fig. 1(*d*) Fig. 2(*d*)	r_p	$\frac{r_{\max}^2 - r_p^2}{r_{\max}^2 - r_2^2}$	$(1-\epsilon)\cdot A_c \cdot \frac{1}{r_o^2}(r_{\max}^2 - r_2^2)$	$(1-\epsilon)\cdot A_c \cdot \frac{2}{r_o}$	$\frac{r_o^2}{2(1-\epsilon)\cdot A_c}\left(\frac{k_p}{k_w}\ln\frac{r_o}{r_{\max}} - \frac{1}{2}\ln\left(1 - \bar{A}_{c,p}\cdot\left(1 - \left(\frac{r_2}{r_{\max}}\right)^2\right)\right)\right)$
Sphere packed bed	Fig. 1(*e*) Fig. 2(*e*)	r_p	$1 - \left(\frac{r_p}{r_{\max}}\right)^3$	$(1-\epsilon)\cdot A_c$	$(1-\epsilon)\cdot A_c \cdot \frac{3}{r_o}$	$\frac{r_o^3}{3(1-\epsilon)\cdot A_c \cdot r_{\max}}\left(\frac{k_p}{k_w}\left(1 - \frac{r_{\max}}{r_o}\right) + (1 - \bar{A}_{c,p})^{-1/3} - 1\right)$

$$\theta_f(\mathrm{Fo}, X = 0) = 1.$$

3.2 Numerical Algorithm. Integrating Eqs. (5)-(6) gives

$$\bar{A}_{c,p}(\mathrm{Fo}, X) = \bar{A}_{c,p,0}(X) + \int_0^{\mathrm{Fo}} \mathrm{Ste}\cdot\mathrm{Bi}\cdot R_r(\mathrm{Fo}, X)\cdot|\theta_f(\mathrm{Fo}, X)|\cdot d\mathrm{Fo} \quad (7)$$

$$\theta_f(\mathrm{Fo}, X) = \exp\left(-\int_0^X \mathrm{NTU}\cdot R_r(\mathrm{Fo}, X)\cdot dX\right) \quad (8)$$

$\theta_f(\mathrm{Fo}, X)$ and $\bar{A}_{c,p}(\mathrm{Fo}, X)$ can be obtained by integrating numerically over space and time. The integration required iteration at each step since R_r is implicitly a function of $\bar{A}_{c,p}$.

From the initial condition, $\bar{A}_{c,p}(\mathrm{Fo} = 0, X) = \bar{A}_{c,p}(0, X)$, $\bar{A}_{c,p}$ increases with time for both charging and discharging processes. As $\bar{A}_{c,p}(\mathrm{Fo}, X)$ approaches 1, the phase change front has crossed the entire PCM region and can no longer move radially. Therefore, the actual heat transfer area will begin to decrease (Fig. 4). The axial position where the PCM is completely solidified/melted is designated as $X_{in}(\mathrm{Fo})$. For $\mathrm{Ste} \ll 1$, the thermal storage capability of that region can be neglected. So the actual heat transfer area can be written as

$$A_{act}(\mathrm{Fo}) = A\cdot(1 - X_{in}(\mathrm{Fo})) \quad (9)$$

The lower limit for the integration in Eq. (8) can then be replaced by $X_{in}(\mathrm{Fo})$.

The dimensionless overall heat transfer coefficient based on the overall heat transfer area is

$$U^*(\mathrm{Fo}) = \int_{X_{in}}^1 \frac{U(X, \mathrm{Fo})}{h_f(X, \mathrm{Fo})} = \int_{X_{in}}^1 R_r(\mathrm{Fo}, X)\cdot dX \quad (10)$$

For a given LHTES system, $\bar{A}_{c,p}(\mathrm{Fo}, X)$ and $\theta_f(\mathrm{Fo}, X)$ are calculated first and then the transient heat transfer rate, thermal storage capacity and molten mass fraction for a thermal discharging process or frozen mass fraction for a thermal charging process are computed using

$$q(\mathrm{Fo}) = \dot{m}_f\cdot c_{p,f}\cdot|\theta_f(\mathrm{Fo}, X = 1) - \theta_f(\mathrm{Fo}, X = 0)|\cdot(T_m - T_{f,in}(\mathrm{Fo})) \quad (11)$$

$$Q(\mathrm{Fo}) = \int_0^{\mathrm{Fo}} q(\mathrm{Fo})d\mathrm{Fo} \quad (12)$$

$$F_r(\mathrm{Fo}) = \frac{Q(\mathrm{Fo})}{A_c\cdot(1-\epsilon)\cdot\rho_p\cdot H_m} = \int_0^1 \bar{A}_{c,p}(\mathrm{Fo}, X)\cdot dX \quad (13)$$

3.3 Model Parameters for Each System. The key point in applying the general model for each system is to determine suitable parameters for each system. The parameters used in the model are listed for each type of LHTES system in Tables 1 and 2. Of the parameters, the equations for Φ were determined using the thermal resistance and those for the other parameters were obtained according to the geometric characteristics of various systems.

3.4 Applicability of the General Model. The model can be used to analyze two dimensional solid-liquid latent heat transfer

Table 2 System parameters (thickness of the wall was neglected)

General model	Fig. 3	$\eta_{p,\max}$	η_f	Number of cells
Flat-plate	Fig. 1(*a*) Fig. 2(*a*)	$y_{\max} = \frac{V}{A}$	$\delta_f = \frac{\epsilon}{1-\epsilon}\cdot\frac{V}{A}$	$\frac{H}{y_{\max} + \delta_f}$
Shell-and-tube with internal flow	Fig. 1(*b*) Fig. 2(*b*)	$r_{\max} = \frac{2\frac{V}{A}}{\left(\frac{1}{\sqrt{\epsilon}} - \sqrt{\epsilon}\right)}$	$r_i = \sqrt{\epsilon}\cdot\frac{2\frac{V}{A}}{\left(\frac{1}{\sqrt{\epsilon}} - \sqrt{\epsilon}\right)}$	$\frac{A_c}{\pi r_{\max}^2}$
Shell-and-tube with parallel flow ($r_2 = 0$)	Fig. 1(*c*) Fig. 2(*c*)	$r_{\max} = 2\frac{V}{A}$	$r_1 = \frac{1}{\sqrt{(1-\epsilon)}}\cdot 2\frac{V}{A}$	$\frac{A_c}{\pi r_1^2}$
Shell-and-tube with cross flow ($r_2 = 0$)	Fig. 1(*d*) Fig. 2(*d*)	$r_{\max} = 2\frac{V}{A}$	$r_{\max} = 2\frac{V}{A}$	1
Sphere packed bed	Fig. 1(*e*) Fig. 2(*e*)	$r_{\max} = 3\frac{V}{A}$	$r_{\max} = 3\frac{V}{A}$	1

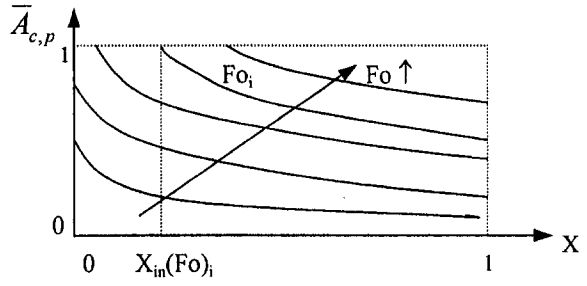

Fig. 4 Typical phase change interface variation

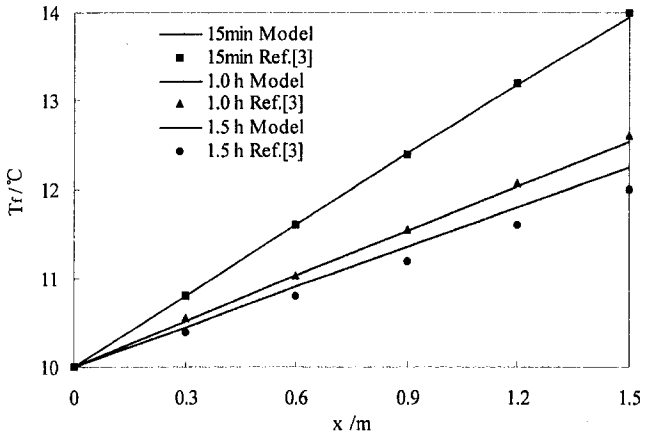

Fig. 5 Comparison of shell-and-tube with result of Cao and Faghri [3]

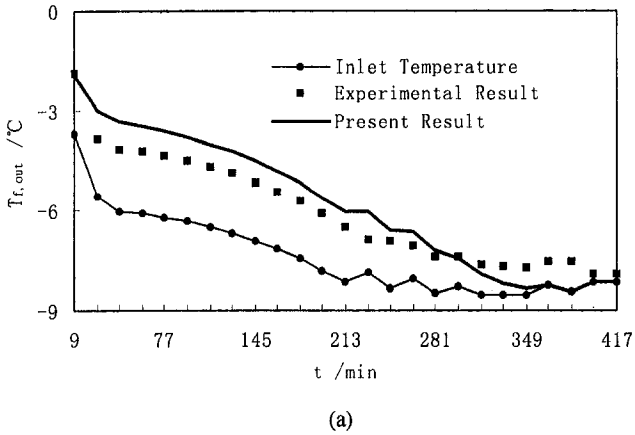

(a)

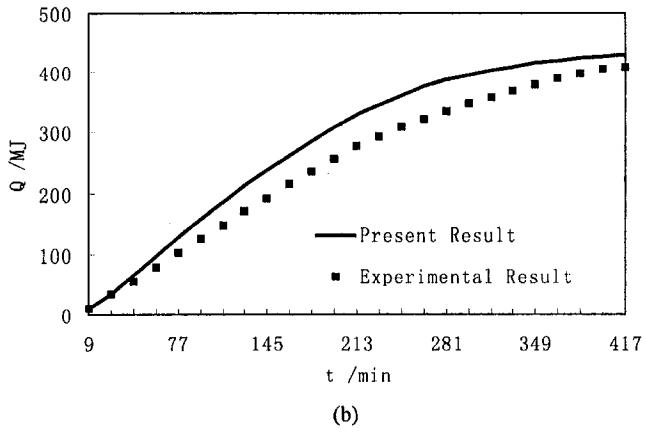

(b)

Fig. 6 Model validation with experimental data (Cool charging process, $\dot{m}_f$ = 3.913 kg s^{-1}, h_f = 83.2 W m^{-2} K^{-1} [13]) (*a*) Comparison of the outlet HTF temperature (*b*) Comparison of the thermal storage capacity

problems with an unknown fluid temperature distribution along the axial direction for all the LHTES systems listed in Tables 1 and 2. The general model can calculate the instantaneous HTF temperature distribution, the instantaneous phase change interface along the axial direction, the instantaneous heat transfer rate, the instantaneous thermal storage capacity, the overall heat transfer coefficient, the effective heat transfer area and the molten/frozen PCM mass fraction. Some of these parameters are important but difficult to measure for monitoring the charging or discharging processes.

The model can also be used when the mass flow rate and/or the HTF inlet temperature vary with time and when the convective

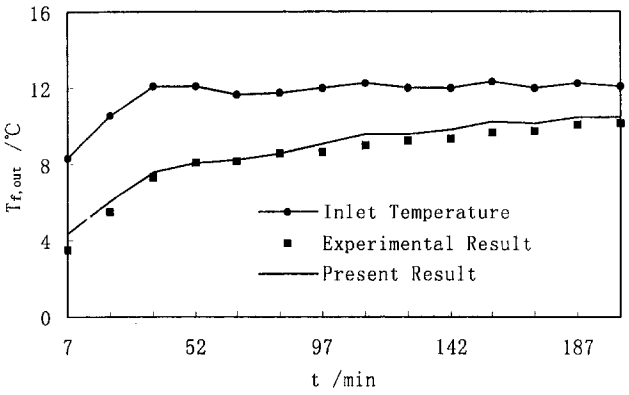

(a)

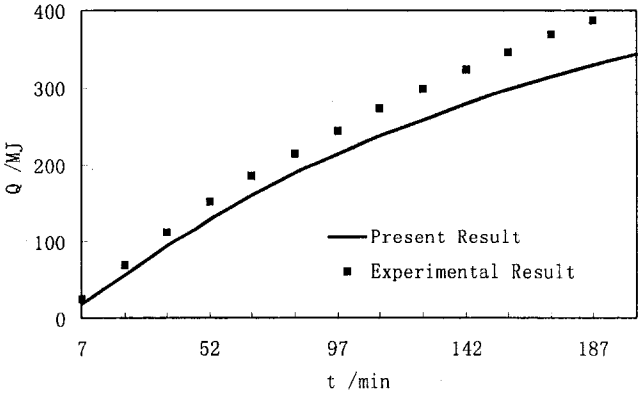

(b)

Fig. 7 Model validation with experimental data (Cool discharging process, $\dot{m}_f$ = 2.613 kg s^{-1}, h_f = 76.2 W m^{-2} K^{-1} [13]) (*a*) Comparison of the outlet HTF temperature (*b*) Comparison of the thermal storage capacity

Table 3 System legends for analysis of system performance (Fig. 9)

	Flat-plate	Shell-and-tube with internal flow	Sphere packed bed
HTF is air	F-A	I-A	S-A
HTF is water	F-W	I-W	S-W

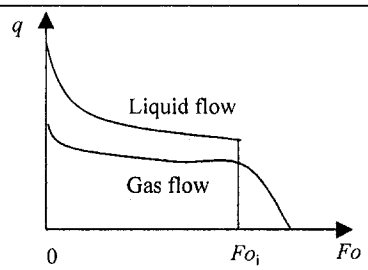

Fig. 8 Heat transfer rate variation in typical LHTES unit

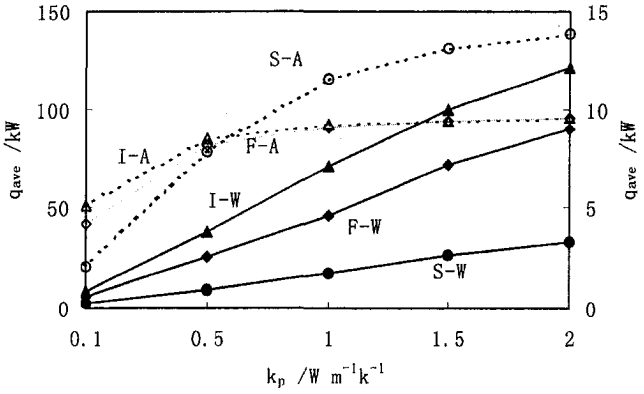

(a)

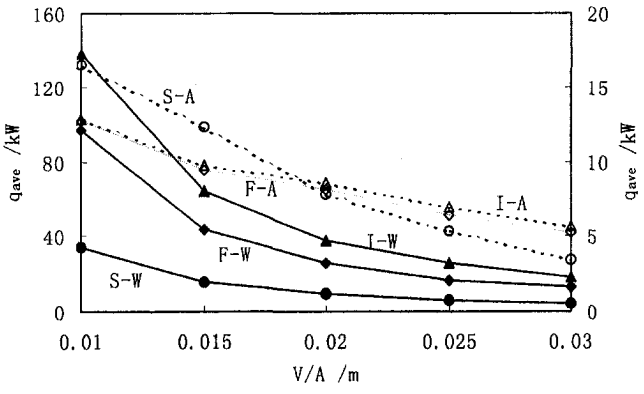

(c)

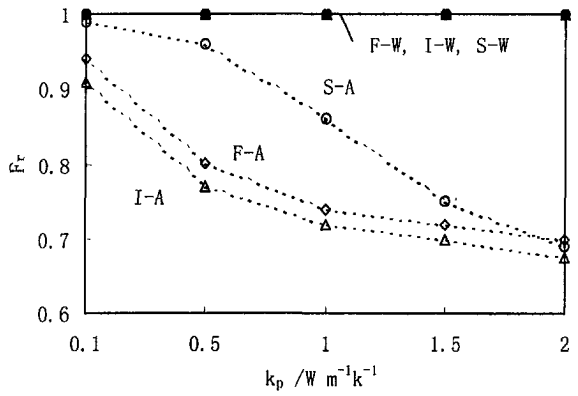

(b)

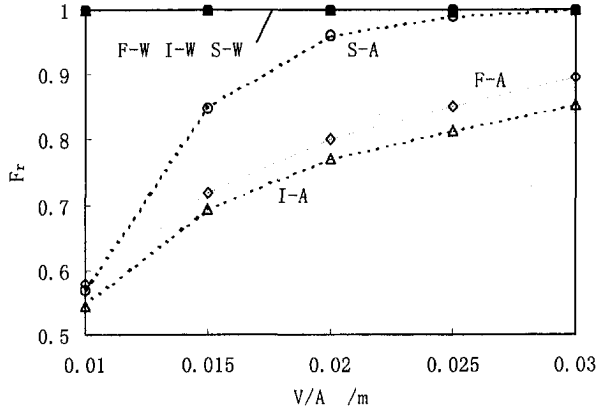

(d)

heat transfer coefficient varies with time or space. Therefore, the method can also include entrance effects. For structures with fins, the convective heat transfer coefficient can be enlarged using [15]

$$h_f^* = \eta_o \cdot \beta \cdot h_f, \quad \eta_o = \frac{A_p + \eta_f A_f}{A_o}, \quad \beta = \frac{A_o}{A_i}, \quad A_o = A_p + A_f$$

Where η_o is the overall efficiency of the finned surface, η_f is the efficiency of a single fin, β is the fin coefficient, A_p is the area of the primary (unfinned) surface of the finned surface, A_f is the fin area, A_o is the overall area of the finned surface and A_i is the overall area of the surface without fins.

The model can also be used for simultaneous charging and discharging processes and for when the PCM is initially partially solidified.

4 Model Validation

The general model was used to simulate the thermal behavior of several types of LHTES systems such as shell-and-tube designs with internal flow, shell-and-tube designs with parallel flow, packed beds with spherical capsules and packed beds with rectangular PCM containers. The simulated results are compared with results in the literature, experimental data and the results of a quasi-steady-state analysis for one-dimensional conditions respectively.

4.1 Comparison with the Results in the Literature. The simulated results for a shell-and-tube LHTES system are compared with the results of Cao and Faghri [3] as shown in Fig. 5. The maximum deviation between them is less than 9.0%.

4.2 Comparison with Quasi-Steady Solution. Ref. [10] studied the phase change process for a single infinite flat-plate, a single cylinder and a single sphere full of PCM with constant wall temperature. The results of the present model are compared with the quasi-steady solution for these one-dimensional phase change problems. The present model was used with the extreme condition that the fluid mass flow rate is large enough so that the temperature difference between the inlet and outlet can be neglected. The relative deviations between the two sets of results range from 0.5–4.5%.

4.3 Comparison with Experimental Data. The model predictions were compared with the experimental data [11] for a spherical packed bed LHTES system. The experimental system had an ice-storage unit packed with ice spheres. The experimental conditions were: r_o = 0.0485 m, r_{max} = 0.0475 m, A_c = 0.785 m^2, ϵ = 0.24, L = 2.5 m, k_w = 12.4 W m^{-1} · K^{-1}, T_m = 0°C and H_m = 334 kJ/kg. Ice was used as the PCM and glycol solution (33 wt. % glycol) was used as the HTF. The computational result and the experimental data are compared for both cool charging and discharging processes in Fig. 6 and Fig. 7. As can be seen for the cool charging process, the thermal storage capacity of the computational result is a little higher than experimental data, while for the cool discharging process, the deviation is opposite. The causes for the lower computational thermal storage capacity are: (1) the sensible heat storage capacities of PCM and HTF are neglected (the final total sensible heat storage capacity for cool charging process is 32 MJ and that for cool discharging process is 35 MJ); (2) the densities of ice and water are slightly different so that the actual phase change front in each capsule is not completely spherical for cool discharging process, which would increase the contact heat transfer and (3) the natural convection in liquid PCM is neglected. While the causes for the higher computational thermal storage capacity are: (1) a little air (about a volume ratio of 5 ~

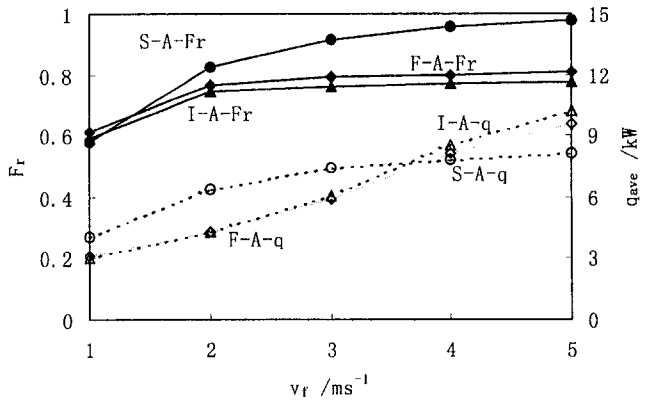

(e)

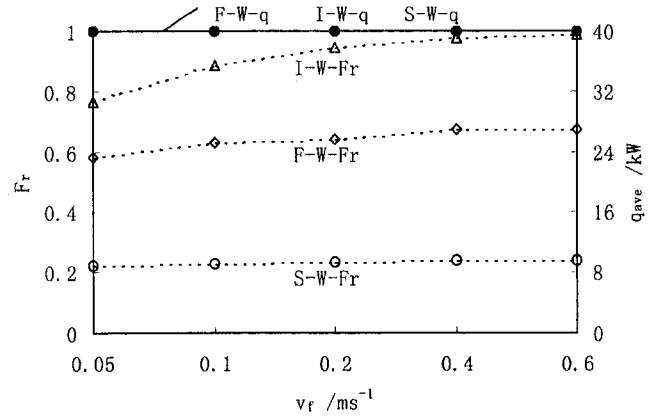

(f)

Fig. 9 Influence of various operating parameters on the thermal performance of LHTES systems (Solid lines refer to the left coordinate and dash lines refer to the right coordinate) (*a*) Influence of k_p on q (*b*) Influence of k_p on F_r (*c*) Influence of *V/A* on q (*d*) Influence of *V/A* on F_r (*e*) Influence of v_f on q and F_r (HTF is air) (*f*) Influence of v_f on q and F_r (HTF is water)

10%) remains in each sphere and (2) as the density of ice is less than that of water, the air layer between the wall and the PCM decreased the heat transfer for the cool charging process. The reasonable agreement between the results using the model and the experimental data shows that the model can be used to predict the thermal performance of various systems.

5 Analysis of Key Factors Influencing the Thermal Performance of LHTES Systems

Analysis of the factors influencing the thermal performance of different LHTES systems can be used to determine the best type of LHTES unit for the system and to optimize the geometric dimensions of the unit.

Consideration of the governing equations show that factors influencing the thermal behavior include the physical parameters of the PCM and HTF and the characteristic parameters of different structures. The key factors are the system shape, type of HTF, PCM thermal conductivity k_p, ratio of cell volume to heat transfer surface area *V/A* and HTF velocity v_f. The influence of these factors on the thermal performance was studied for the various systems listed in Table 3. For a given LHTES system in Fig. 3, relating known parameters are

PCM: $T_m = 20°C$, $H_m = 200$ kJ kg^{-1}, $c_{p,p} = 2.0$ kJ kg^{-1} K^{-1}, $\rho_p = 1000$ kg m^{-3}

LHTES unit: $A_c = 1$ m^2, $L = 2$ m, $\epsilon = 0.35$ (For flat-plate system: $W = 1$ m)

Operating condition: (a) HTF is air: $T_{f,in} = 10°C$; (b) HTF is water: $T_{f,in} = 15°C$

The convective heat transfer coefficients for the various structures were obtained from the formula in Refs. [12–15]. Since the heat transfer rate varies during the phase change process (Fig. 8) and the effective heat transfer area decreases during operation (Fig. 4), the average heat transfer rate

$$q_{ave} = \frac{\int_0^{\mathrm{Fo}_i} q(\mathrm{Fo})d\mathrm{Fo}}{\mathrm{Fo}_i} \tag{14}$$

and the molten/frozen mass fraction when the effective heat transfer area began to decrease, $F_r(\mathrm{Fo}_i)$, are used to present the thermal performance.

The influence of k_p on q_{ave} and F_r is shown in Fig. 9(*a*) and (*b*). When air is used as the HTF in flat-plate and shell-and-tube systems with internal flow, q_{ave} increases while F_r decreases as k_p increases for $k_p < 0.6$, while for $k_p > 0.6$, the influence of k_p is not significant. For the sphere packed bed structure, q_{ave} increases while F_r decreases as k_p increases. For water as the HTF, q_{ave} increases as k_p increases and F_r is about 100% for all the systems, which indicates that the effective heat transfer area does not decrease.

The influence of *V/A* on q_{ave} and F_r is shown in Fig. 9(*c*) and (*d*). The results show that for all the structures, q_{ave} decreases and

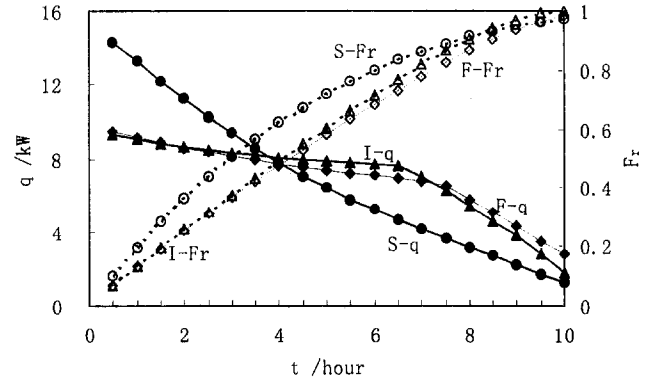

(a)

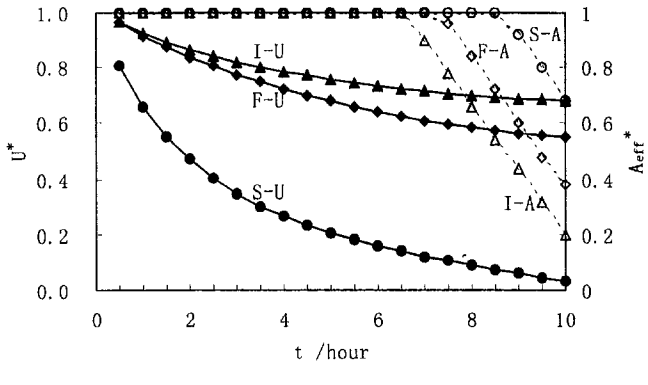

(b)

Fig. 10 Thermal behavior of different LHTES structures—HTF is air (k_p = 0.5 W m^{-1} K^{-1}, *V/A* = 0.02, v_f = 4 ms^{-1}, solid lines refer to the left coordinate and dash lines refer to the right coordinate) (*a*) Variation of heat transfer rate and frozen mass fraction (*b*) Variation of dimensionless overall heat transfer coefficient and effective heat transfer area

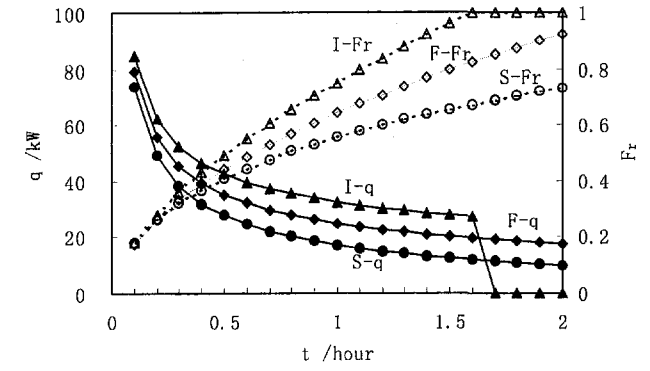

(a)

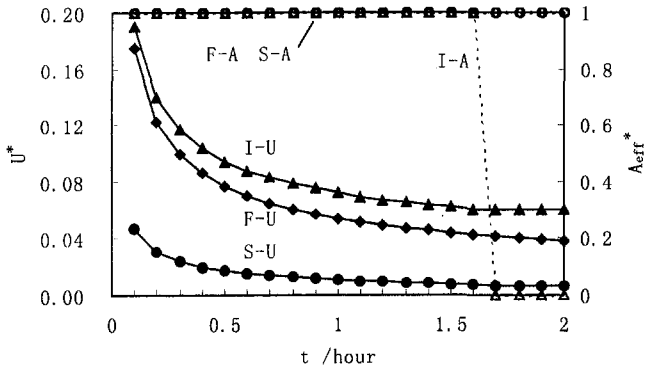

(b)

Fig. 11 Thermal behavior of different LHTES structures—HTF is water (k_p = 0.5 W m^{-1} K^{-1}, V/A = 0.02, v_f = 0.2 ms^{-1}, solid lines refer to the left coordinate and dash lines refer to the right coordinate) (*a*) Variation of heat transfer rate and frozen mass fraction (*b*) Variation of dimensionless overall heat transfer coefficient and effective heat transfer area

Table 4 Calculated system parameters (Figs. 10 and 11)

	Flat-plate	Shell-and-tube with internal flow	Sphere packed bed
$\eta_{p,max}$	0.02	0.0364	0.06
η_f	0.0108	0.0215	0.06
Cell number	33	240	1

F_r increases as V/A increases for air as the HTF and q_{ave} decreases as V/A increases and F_r remains near 100% for water as the HTF. As can be seen, the influence of V/A on q_{ave} and F_r is more significant for sphere packed bed than for flat-plate system and shell-and-tube system with internal flow.

The influence of v_f on q_{ave} and F_r is shown in Fig. 9(*e*) and (*f*). For air as HTF, q_{ave} increases and F_r does not vary significantly as v_f increases, while for water as HTF, v_f has little influence on either q_{ave} and or F_r.

The conclusions can be summarized as:

(1) When k_p or v_f increases or V/A decreases, q_{ave} will increase and F_r will decrease.

(2) Under most operating conditions of this example, the effective heat transfer area decreases during the phase change process for air as the HTF, but does not change for water as the HTF.

(3) For the systems analyzed, increasing k_p or decreasing V/A will increase the heat transfer rate significantly. For air as the HTF, increasing v_f will increase the heat transfer rate significantly, while for water as the HTF, increasing v_f will not increase the heat transfer rate significantly.

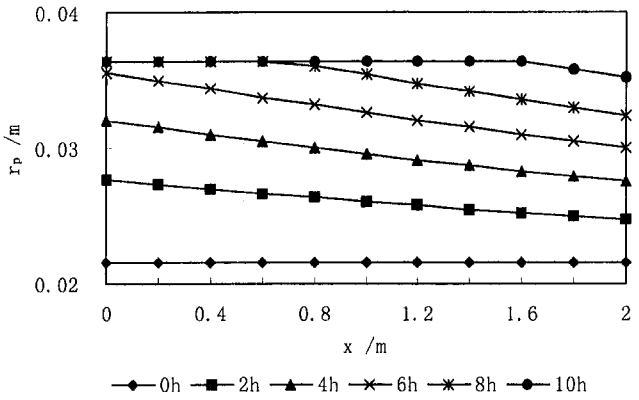

(a)

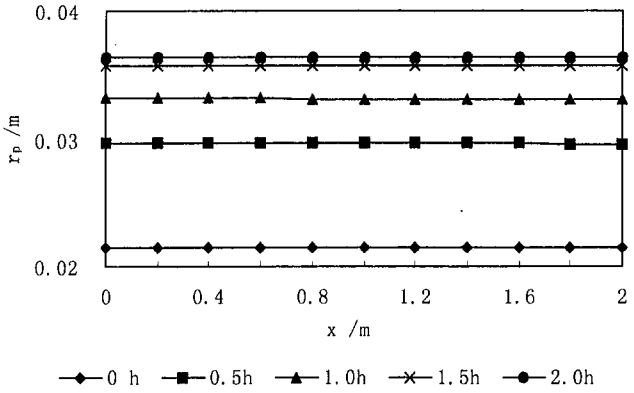

(b)

Fig. 12 Variation of phase change interface distribution in a shell-and-tube system with internal flow (*a*) HTF is air (k_p = 0.5 W m^{-1} K^{-1}, V/A = 0.02, v_f = 4 ms^{-1}) (*b*) HTF is water (k_p = 0.5 W m^{-1} K^{-1}, V/A = 0.02, v_f = 0.2 ms^{-1})

The instantaneous thermal behavior including the timewise variation of the heat transfer rate, the molten/frozen mass fraction, the dimensionless heat transfer coefficient and effective heat transfer area for the various systems for both air and water as the HTF are presented in Figs. 10 and 11. The values of the overall performance for each system are listed in Table 4. The shell-and-tube system with internal flow has the best performance for these conditions. In addition, the results indicate that the decreasing trend of heat transfer area is approximately linear with air as the HTF. The timewise variation of phase change interface profile for the shell-and-tube system with internal flow is presented in Fig. 12. The PCM solidifies/melts faster near the entrance than near the exit, which reduces the effective heat transfer area for air as the HTF. For water as the HTF which has far less NTU than the air system (for this case, NTU for water system is 0.17 and NTU for air system is 18.6), according to Eq. (8), water temperature would vary little along the axial direction, resulting in the phase change interface varying little from the entrance to the exit. Therefore, the phase change interface along the axial direction is nearly parallel to the wall as time progresses.

6 Conclusions

The common features of various LHTES systems in practical applications were used to develop a general heat transfer model which is valid for variable flow rates and variable inlet HTF temperatures, and finned structures. The general model can be used to simulate the thermal behavior under various operating condi-

tions. The model was verified by experimental results in the literature. In addition, the influence of key factors including the type of system, type of HTF, PCM thermal conductivity, ratio of cell volume to the heat transfer surface area, and the HTF velocity on the thermal behavior of each system was studied in detail. The results show that these key factors influence the thermal performance of LHTES systems in different ways. The general model provides guidance for system selection and optimization and performance simulation of solid-liquid LHTES systems.

Acknowledgment

This work was supported by the Natural Science Foundation of the People's Republic of China.

References

1 Brousseau, P., and Lacroix, M., 1996, "Study of the Thermal Performance of a Multi-Layer PCM Storage Unit," *Energy Convers. Mgmt.,* Vol. 37, No. 5, pp. 599–609.

2 Cao, Y., and Faghri, A., 1991, "Performance Characteristics of a Thermal Energy Storage Module: A Transient PCM/Forced Convection Conjugate Analyses," *Int. J. Heat Mass Transfer,* Vol. 34, No. 1, pp. 93–101.

3 Cao, Y., and Faghri, A., 1989 , "A Numerical Analysis of Stefan Problems for Generalized Multi-Dimensional Phase-Change Structures Using the Enthalpy Transforming Model," *Int. J. Heat Mass Transfer,* Vol. 32, No. 7, pp. 1289–1298.

4 Cao, Y., and Faghri, A., 1992, "A Study of Thermal Energy Storage Systems with Conjugate Turbulent Forced Convection," *Journal of Heat Transfer,* Vol. 114, November, pp. 1019–1027.

5 Esen, M., and Durmus, A., 1998, "Geometric Design of Solar-Aided Latent Heat Storage Depending on Various Parameters and PCMs," *Solar Energy,* Vol. 62, No. 1, pp. 19–28.

6 Egolf, P., and Frei, B., 1997, "A Simplified Model to Describe Heat Transfer by Free Convection in a Water Storage Tank Containing Spherical Phase Change Material Capsules," Proc. of 7th International Conference on Thermal Energy Storage, Sapporo, Japan, pp. 145–150.

7 Homma, T., Watanabe, K., et al., 1997, "Heat Characteristics of Spherical Latent Heat Storage Capsules," Proc. of 7th International Conference on Thermal Energy Storage, Sapporo, Japan, pp. 313–318.

8 Arnold, D., 1991, "Dynamic Simulation of Encapsulated Ice Stores," *ASHRAE Trans.,* Vol. 96, No. 1, pp. 1103–1110.

9 Arnold, D., 1991, "Laboratory Performance of an Encapsulated Ice Stores," *ASHRAE Trans.,* Vol. 97, No. 2, pp. 1170–1177.

10 Zhang, Y. P., Hu, H. P., Kong, X. D., and Su, Y. H., 1996, "Latent Thermal Energy Storage-Theory and Application," China Science and Technology Book Company (in Chinese).

11 Li, H., 1997, "The Experimental Research on the Ice Storage Equipment's Utility of Heat Transfer," Thesis of Master Degree of Tsinghua University in China (in Chinese), (May).

12 Rohsenow, W. M., 1985, "Handbook of Heat Transfer Fundamentals," pp. 108, McGraw-Hill.

13 Rohsenow, W. M., 1985, "Handbook of Heat Transfer Applications," pp. 445, McGraw-Hill.

14 Kays, W. M., and Crawford, M. E., 1980, "Convective Heat and Mass Transfer," pp. 248–252, McGraw-Hill.

15 Incropera, F. P., and Dewitt, D. P., 1996, "Fundamentals of Heat and Mass Transfer" (Fourth Edition), pp. 378–380, John Wiley & Sons.